A laboratory-scale automated vacuum-assisted device for coating of cellulose nanofibrils onto paper

SANDRO ZIER, ZECHARIAH HOEFT, JAMIESON SNAPE, DOUGLAS BOUSFIELD, AND CAITLIN HOWELL

ABSTRACT: An automated vacuum-assisted coating system was developed to deposit cellulose nanofibril (CNF) layers onto paper substrates, simulating potential industrial geometries while allowing precise control of web speed (10–20 m/min), vacuum time (up to 30 s), and applicator gap (0.5–0.9 mm). Vacuum assistance makes it possible to obtain coat weights over 5 g/m² in a single pass and increases solids after coating from less than 10% to over 28%–30%, reducing drying demand by more than 60%. Coat weights were tuned from 6 to over 11 g/m² by varying suspension solids (0.4–0.6 wt%), line speed, and filtration length (20–40 mm), with strong agreement between experimental data and model predictions. Barrier testing showed Kit test values for double folded samples of 9–12 and Gurley air resistances above 4×10^4 s once coat weights exceeded 7 g/m². Comparable performance was achieved with lower fines content CNF (60%) by increasing coat weight, providing technical flexibility and cost advantages for industrial scale-up.

Application: This unique method for coating CNF onto paper produces high enough coat weights in a single pass to obtain good barrier properties.

A layer of cellulose nanofibrils (CNFs) on a base paper has the potential to generate a new grade of paper that has high utility in food packaging applications and can replace plastics by providing functionality, scalability, and environmental sustainability. The CNFs are produced through mechanical disintegration processes such as refining, grinding, or high-pressure homogenization [1,2]. The CNFs typically exhibit fibril widths of 5–50 nm and lengths extending to several micrometers. Their surfaces are densely populated with hydroxyl groups, rendering them highly hydrophilic [3,4]. Industrial-scale production of CNFs has already been established [5], and their cost remains relatively competitive compared with other bio-based alternatives [6]. Importantly, CNFs retain desirable mechanical properties, including tensile strength and flexibility, making them suitable for food packaging applications [7]. In addition, CNFs can be formed into thin films that provide excellent barrier performance against oil, grease, and oxygen [8], properties considered essential for packaging materials [9–11]. These films are even viable after folding [12] and can be used as the basis for other useful add-on coatings, such as mycelial films.[13]

A practical and cost-effective strategy for utilizing CNFs in packaging applications is to apply them as coatings on paper substrates, where the paper provides mechanical stability and the CNF layer imparts barrier properties [4,14]. Despite this potential, CNF coatings present significant processing challenges due to their strong water affinity and complex rheology. To achieve the barrier levels required for food packaging, such as low oxygen permeability and resistance to oil and grease, coat weights of at least 10–15 g/m² are typically necessary [15]. However, the high aspect ratio of CNFs, their ability to form entangled networks in suspension, and their interactions with water hinder the deposition of such coat weights in a single step; many have reported the need for multiple coating operations to obtain significant coverage [16–27].

Near moving boundaries, fibers form dense rotating flocs, or "rollers," that compact spacing and release water into the bulk, leading to a water-rich layer; this effect intensifies under high shear or narrow gaps in industrial rod and blade coating systems [28]. While alternative methods such as slot-die coating can deliver higher coat weights [20,29-33], they require processing CNF suspensions at low solids, which results in high energy costs related to the need for thermal drying [27,30]. Consequently, advancing scalable and efficient coating processes capable of achieving the required CNF coat weights in a single step remains critical to enabling the widespread adoption of CNF-based packaging.

Recent work has shown the benefits of a CNF layer on paper. The CNF layers not only generate high oil and grease resistance [34], they also help barrier coatings to be more effective [35,36]. The CNF layers can give good oxygen barrier properties, especially when combined with a barrier coating [36], and they can help in the recycling of barrier

coated products [37]. Recently, some research groups have found that it is possible to use filtration methods to apply CNFs to paper surfaces [12,38]. However, benchtop batch trials need to be scaled up to continuous processes before any large-scale production is possible. One method to do so is the use of hand-drawn, single-step vacuum-assisted coating [39], which has been shown to create uniform CNF layers of up to 28 g/m² in a single step.

In this work, the next step toward scale-up is demonstrated through the development of an automated vacuum-assisted coater designed to mimic a possible industrially relevant process, enabling precise control over web speed, vacuum length and duration, and gap distance. The system can reliably increase CNF coat weights to levels that provide good barrier properties, explain the mechanisms that enable this improvement, and provide predictive capability for coat weight outcomes. By systematically varying operating parameters in a controllable way, multiple levers including solids concentration, vacuum conditions, and gap settings can be used to tune coat weight, and that different routes to the same coat weight may yield similar or distinct barrier properties. Finally, it was found that equivalent barrier performance can be achieved even with low grade CNF, offering a pathway to reduce production costs while maintaining functionality. Together, these findings advance the transition of CNF coatings from benchtop feasibility toward scalable industrial application.

METHODS AND MATERIALS

Paper was supplied by Kruger (Krukraft, Kruger Inc.; Montreal) with a basis weight of 49 g/m². The CNF was produced at the University of Maine Process Development Center (PDC) in Orono, ME, USA, using a refiner as described in other publications. The CNF can be refined to different grades and is characterized by a fiber size analyzer (MorFi, Techpap SAS; Giéres, France) based on percent fines. A CNF at 90% fines is the standard material, but results at 60% and 80% fines are also reported here.

An automated vacuum-assisted rod coater was constructed to replicate potential industrial coating conditions while maintaining laboratory-scale control and flexibility. The design replaces the benchtop configuration, where the rod was moved manually, with a stationary stainless-steel metering rod (Rod 20) that rotates in place above a moving web platform. Web motion is driven by a stepper-motor linear actuator, allowing precise programming and reproducible adjustment of web speed controlled by an Arduino Uno R4 (Arduino; Monza, Italy) between 3 and 50 m/min. The coating trough was designed to steadily deliver suspension during web movement and make use of an increased filtration time, ensuring consistent material delivery at the coating interface. Process parameters, including web speed, vacuum length, vacuum time, and the gap distance between substrate and rod, are independently programmable or designable, enabling systematic variation and precise control. Together, these features make the coater directly analogous to potential commercial rod and blade systems, with improvements toward automation, continuous operation, and speed control, while remaining suitable for controlled laboratory-scale studies.

After the paper was coated, it was dried at 90°C for 90 min, with the CNF coated side against a stainless-steel sheet weighted on the backside with a mesh 40 stainless-steel mesh. A weight applying a pressure of around 1.0 kN/m² was placed on top to simulate drying pressures in the drying section of a paper machine. The samples were then tested with the standard air permeability test, TAPPI Standard Test Method T 460 "Air resistance of paper (Gurley method)," and for grease resistance with TAPPI T 559 "Grease resistance test for paper and paperboard" (Kit test)." Two types of tests were conducted: one in which the samples were laid flat and another in which the samples had been folded twice orthogonally to create a single point at which the coating had undergone folding in two separate directions (double folded). In the following results, samples that were subjected to double folded tests are specifically indicated; a lack of specific indication signifies that only flat testing was conducted.

Coat weight model development

The coating model was designed to capture the build-up of CNF deposition during vacuum-assisted coating. Two dominant mechanisms were considered: filtration through the substrate under vacuum and gap-limited deposition determined by the rod clearance.

The coat weight obtained by filtering the CNF onto the paper C_f can be calculated using the filtration equation as follows:

$$C_f = \sqrt{\frac{2\Delta P t C_s}{\mu \alpha}} \quad [1]$$

where ΔP is the applied pressure drop (Pa); μ is the liquid phase viscosity (Pa•s); α is the specific cake resistance (kg/m) of the CNF layer; C_s is the concentration of solids in the suspension (kg/m³); and t is the residence time under vacuum before the rod(s). This equation assumes that the substrate offers no resistance to flow, but this can be modified if the permeability of the paper is measured and is important. The specific filter cake resistance used was 3.0 x 10^{12} m/kg; this value is lower that what others have measured for thick filter cakes, but it gives a reasonable description of the behavior of this coating system. The C_s depends on the solids of the CNF suspension. For example, 0.5% solids gives C_s as 5 kg/m³. Throughout all trials, the applied pressure drop was consistently maintained at a level of 25 kPa.

In addition to filtration, a geometric deposition term was included to account for liquid entrained by the web through the gap. This was modeled as follows:

$$C_g = C_s h \quad [2]$$

where C_g is the dry mass per unit area from the gap, and h is the rod–substrate gap. This term assumes the gap height directly fixes the retained wet film thickness.

The total coat weight reported by the model is the sum of the filtration-derived mass (Eq. 1) and the geometric gap mass (Eq. 2). The formulation thus combines process-dependent deposition (vacuum pressure, viscosity, concentration, residence time) with purely geometric deposition (gap).

RESULTS AND DISCUSSION

The design and operating principle of the system are shown in **Fig. 1**. The assembled system as a CAD drawing is depicted is Fig. 1a, which integrates a stationary applicator and dosage rod with a controllable web transport mounted on linear rails. This configuration reproduces potential industrial coating geometries while enabling precise laboratory-scale experimentation. The system is fully automated and allows direct control of web speed, vacuum length, vacuum time, and applicator gap parameters that are critical for scaling to continuous production. Figure 1b shows a picture of the build systems. Figure 5c illustrates the coating sequence: a CNF suspension is applied to the paper ahead of the dosage rod that is experiencing vacuum. The rod meters the film to some thickness while the moving substrate transports the suspension over further vacuum sections. Here, filtration removes water and consolidates the CNF filter cake onto the paper surface. Together, these features establish a coater that not only mimics the potential scaled-up industrial processes but also provides the fine control necessary for mechanistic studies, predictive modeling, and process optimization.

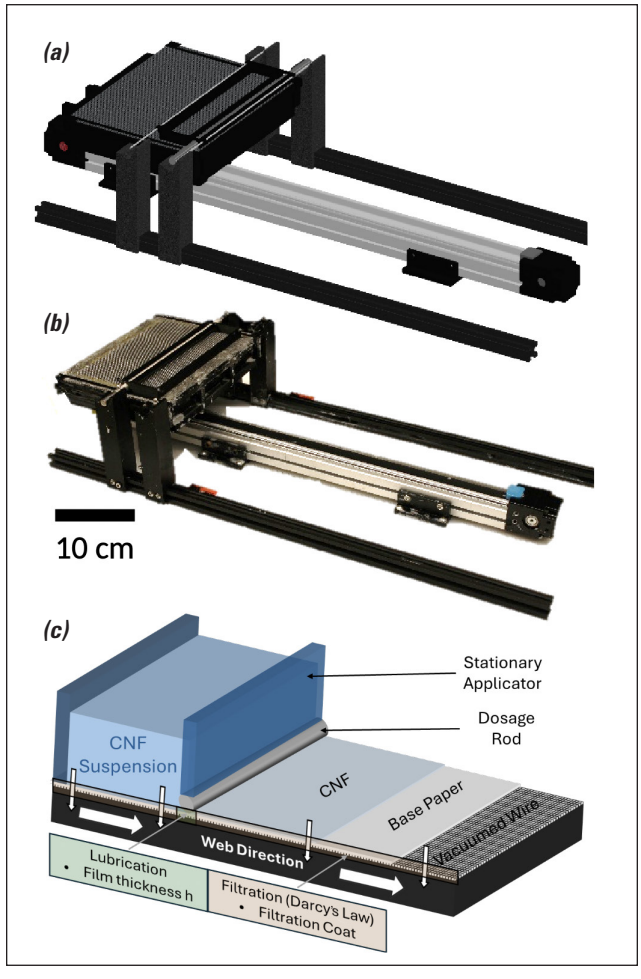

1. Automated vacuum-assisted coating system: (a) assembled coater with stationary applicator, dosage rod, and linear web transport; (b) photograph of the coater; and (c) schematic of the coating process showing CNF suspension application, metering by the dosage rod, vacuum wire, and formation of a CNF filter cake on the paper substrate.

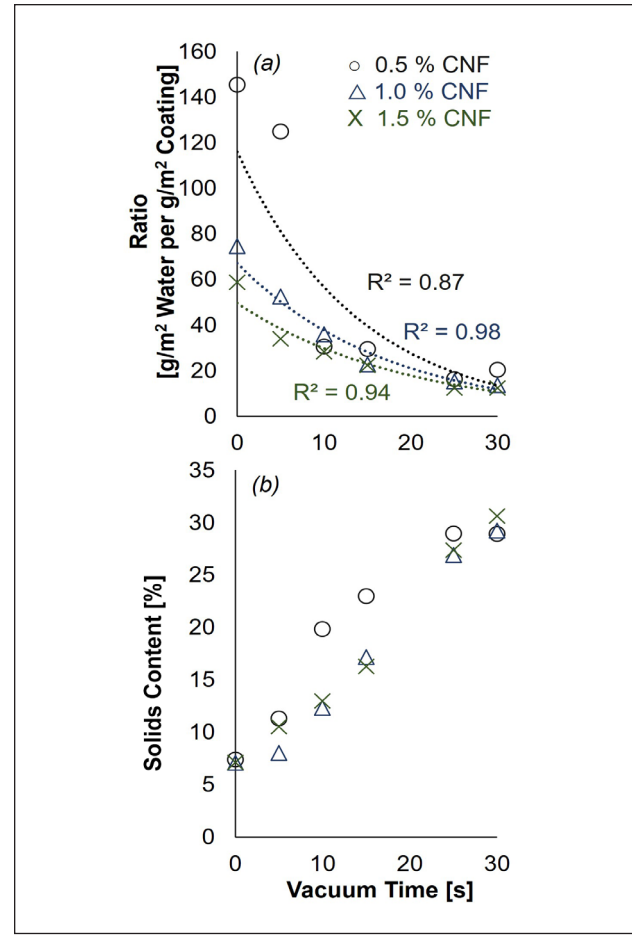

2. Effect of vacuum time on dewatering of cellulose nanofibril (CNF) suspensions with different initial solids contents (0.5 wt%, 1.0 wt%, and 1.5 wt% with rod gap 0.7 mm, and vacuum level of 25 kPa): (a) ratio of water removed per unit CNF coat weight as a function of vacuum time, with dotted lines showing fitted trends, and (b) resulting solids content of the coating layer as a function of vacuum time (R^2: coefficient of determination).

One critical issue for this coating method is the solids of the paper and CNF layer after coating and before drying, because that determines the drying energy required. **Figure 2** provides a direct demonstration of how opera-

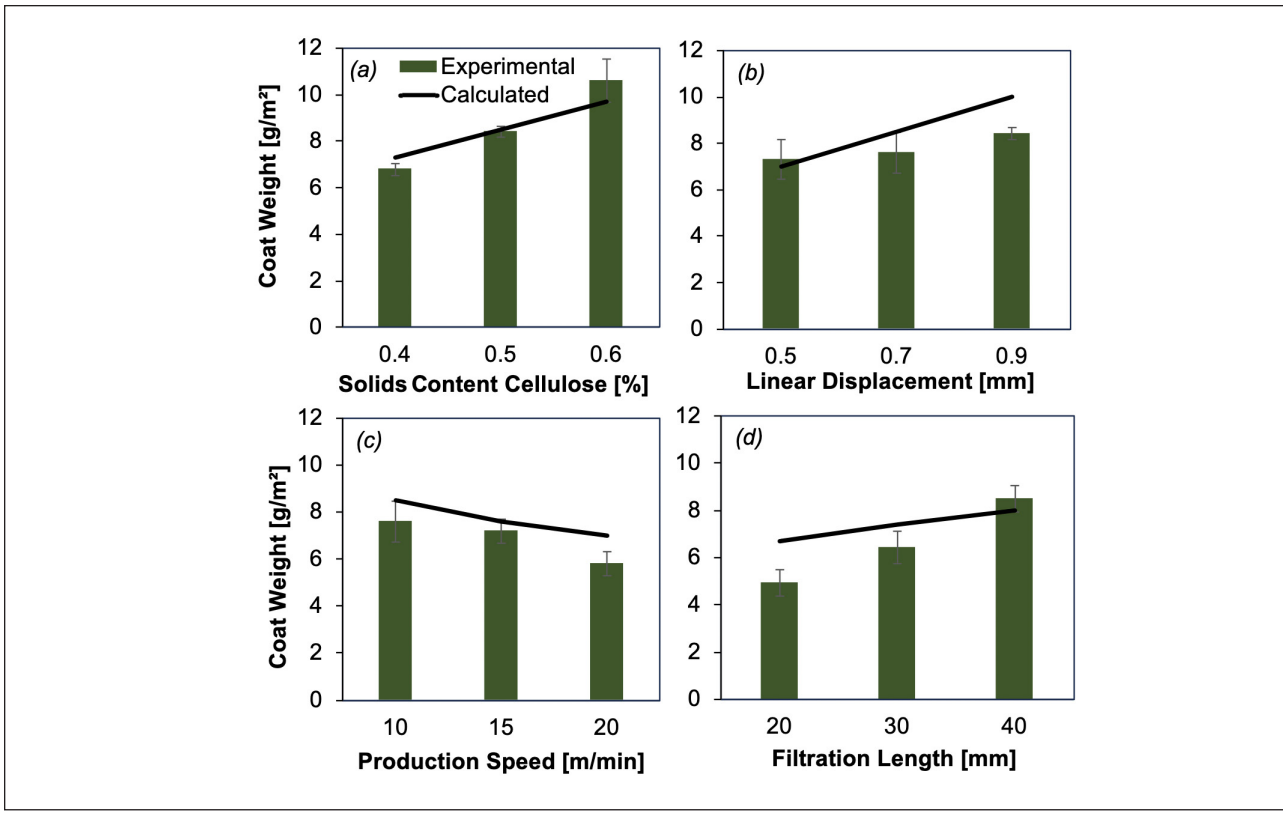

3. Influence of process parameters on CNF coat weight with experimental data (bars, mean ± standard deviation) and model predictions (black lines): (a) effect of initial solids content (0.4 wt%–0.6 wt%); (b) effect of applicator displacement (0.5–0.9 mm); (c) effect of web speed (10–20 m/min; and (d) effect of filtration length (20–40 mm).

tional parameters translate into measurable differences in water removal and final solids concentration, linking the apparatus design to its process-level impact.

Figure 2 presents the effect of total vacuum time on water removal and solids concentration for coatings applied with different initial CNF suspension solids contents using equal applied suspension volumes; this vacuum time is the time before and after the paper is in contact with the rod metering step. Figure 2a shows that the ratio of water removed per unit CNF deposited decreases with increasing vacuum time for all suspensions, though the absolute values depend on initial solids. The 0.5 wt% suspension requires removal of substantially more water per gram of CNF, starting above 140 g/m² water per g/m² CNF, while the 1.5 wt% suspension begins at less than half this ratio, reflecting its lower initial water burden. Despite these differences, all three suspensions converge toward similar ratios (< 20 g/m² water per g/m² CNF) after ~30 s of vacuum, indicating that extended vacuuming levels out the initial compositional differences by effectively draining excess water. Figure 2b shows the resulting solids content of the coated layer. Because identical suspension volumes were applied, the final solids content rises more steeply for higher initial concentrations, reaching ~30% for the 1.5 wt% suspension at 30 s, compared to ~29% and ~28% for the 1.0 wt% and 0.5 wt% suspensions, respectively. These results show the dual role of vacuum time and feed concentration in determining coating efficiency: longer vacuum time increases solids content regardless of feed, while higher initial solids amplify this effect by reducing the relative water load. Importantly, this has direct implications for scalability. Industrial competitiveness of CNF coatings depends on minimizing energy-intensive drying steps; starting with higher solids suspensions reduces the absolute water removal required, while vacuum dewatering rapidly drives the coating into the >28%–30% solids range where conventional thermal drying processes become efficient. Thus, combining optimized feed concentration with vacuum-assisted drainage provides a practical pathway toward lowering energy costs and achieving industrially viable CNF barrier coatings on paper.

Figure 3 presents the effect of four independent process parameters on CNF coat weight, with experimental data compared against model predictions. In all panels, the *y*-axis represents the dry coat weight (g/m²), while the *x*-axis shows the parameter under investigation. Importantly, previous work has shown that without vacuum, rod or blade coating CNF yields coat weights of only around 2 g/m² [17,39,40]. In Figure 3a, the base parameters include a filtration length of 40 mm, a linear distance of 0.7 mm, and a production speed of 10 m/min. The data in Fig. 3a demonstrates the relationship between coat weight and initial solids content (0.4 wt%–0.6 wt%) when a vacuum is ap-

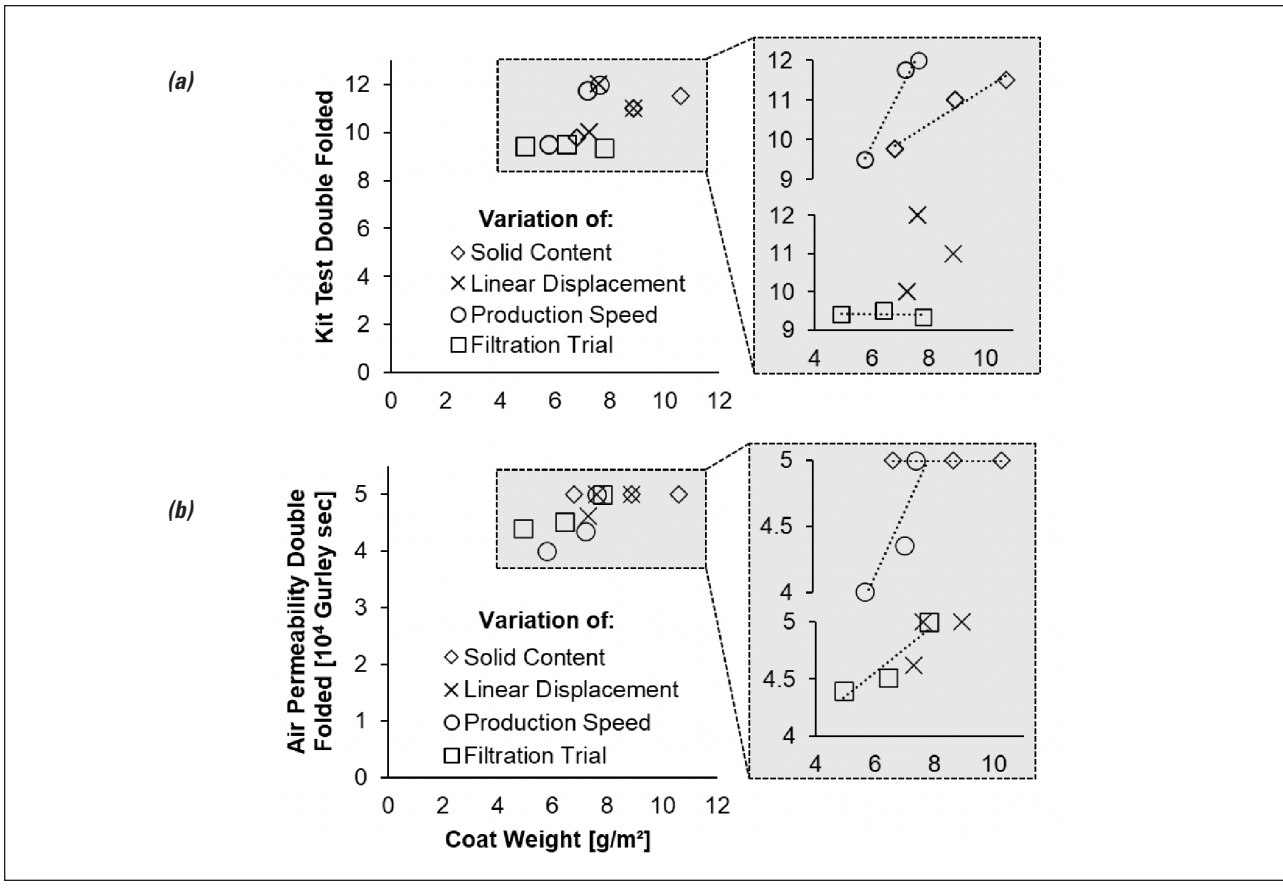

4. Relationship between coat weight and barrier performance; a darker color indicates a higher value of solid content, displacement, speed, or length: (a) double-folded Kit test values as a function of coat weight, and (b) double-folded air permeability (Gurley seconds × 10^4) as a function of coat weight. Data points are grouped according to the parameter adjusted to achieve the coat weight: solids content (diamonds), linear displacement (crosses), production speed (circles), and filtration length (squares).

plied, showing a nearly linear increase in coat weight from approximately 7 g/m² at 0.4 wt% to over 10 g/m² at 0.6 wt%. In Fig. 3b, the base configuration consists of a solids content of 0.5%, a filtration length of 40 mm, and a production speed of 10 m/min. This figure details the effect of applicator displacement, revealing that increasing the displacement from 0.5 to 0.9 mm results in an increase in coat weight by approximately 2 g/m². This increase is attributed to a higher volume flowing through the gap between the rod and the paper. In Fig. 3c, the parameters remain consistent with a solids content of 0.5%, a filtration length of 40 mm, and a linear distance of 0.7 mm. The parameter under investigation is web speed, which indicates that raising the speed from 10 to 20 m/min results in a decrease in coat weight from approximately 7.5 g/m² to around 6 g/m², reflecting the reduced residence time available for dewatering at higher speeds. Lastly, Fig. 3d features a solids content of 0.5%, a production speed of 10 m/min, and a linear distance of 0.7 mm. This experiment shows the influence of filtration length before the rod, revealing an increase in coat weight of nearly 4 g/m² when the vacuum section is extended from 20 to 40 mm and emphasizing the significance of prolonged dewatering times in enhancing deposition.

The model results do a reasonable job at capturing the correct trends and give the correct behavior. The model tends to overestimate the influence of rod gap (Fig. 3b) and underestimate the role of vacuum time (Fig. 3d). This can be caused by several factors or assumptions that were made in the simple model, such as neglecting the flow resistance of the base paper, the extra pressure due to the coating flow field, and the assumption of a constant filter cake resistance coefficient.

The results in Fig. 3 demonstrate that coat weight is not determined by a single factor but can be tuned through multiple independent levers, including suspension solids content, applicator geometry, web speed, and vacuum length. In general, accurate tendencies between experimental and calculated values can be observed. Nonetheless, to further improve the model, especially for the linear displacement trial displayed in Fig. 3b, a more complicated approach can be applied. By enabling reliable forecasting of coat weight outcomes, the model provides a tool for process optimization and accelerates the pathway toward industrial implementation of CNF coatings in packaging.

Figure 4 shows the relationship between coat weight and functional barrier properties, highlighting how differ-

ent process routes to achieve a given coat weight can yield either similar or distinct barrier outcomes. In Fig. 4a and Fig. 4b, the *x*-axes represent measured coat weight (g/m²), while the *y*-axes show performance metrics: Fig. 4a plots oil and grease resistance (double-folded Kit test value), and Fig. 4b shows air impermeability (double-folded Gurley seconds × 10^4). Across all conditions, increasing coat weight is associated with higher barrier performance, but the pathway used to reach a given coat weight influences the outcome. For oil and grease resistance (Fig. 4a), most samples cluster around Kit values of 9–12 once coat weights exceed ~7 g/m², regardless of how the coat weight was achieved. This suggests that different parameter adjustments can converge on similar grease-resistance levels, provided sufficient CNF is deposited. By contrast, the air permeability results (Fig. 4b) reveal subtle differences: while high coat weights (> 7 g/m²) generally yield Gurley values above 4 × 10^4 s, samples obtained by increasing solids content or linear displacement show slightly better air impermeability than those produced by modifying filtration length or production speed. These results demonstrate that coat weight is a necessary, but not sufficient, predictor of performance: although multiple process adjustments can produce coatings with similar mass loadings, the microstructure and uniformity of the deposited CNF layer differ depending on the varied parameter, leading to differences in barrier performance. This finding highlights the importance of not only targeting a specific coat weight but also considering the process route used to achieve it, as different routes may converge on comparable grease resistance but diverge in air barrier properties

Figure 5 shows the effect of fines content of the CNF used as measured by a fiber size analyzer and coat weight on barrier performance, with flat Kit test values shown in Fig. 5a and flat air permeability in Fig. 5b. In both cases, the *x*-axis represents coat weight (g/m²), while the *y*-axis shows either grease resistance (Kit number) or air impermeability (Gurley seconds × 10^4). Each color represents the fines content level of the CNF used (60%, 80%, and 90%).

For the Kit test in Fig. 5a, performance increases consistently with both coat weight and fines content. The fitted curves (R^2 = 0.90–0.99) confirm that higher fines fractions reduce the coat weight required to achieve a given Kit value. For example, a target Kit level can be reached at lower coat weights when fines content is high (90%), whereas similar performance at 60% fines requires applying thicker coatings. This highlights that grease resistance is sensitive to both CNF fines fraction and coat weight, with coat weight partially compensating for lower fines.

For flat air permeability in Fig. 5b, the same general trend is observed, but the magnitude of improvement is less pronounced, consistent with the lower sensitivity of Gurley testing compared to the Kit test. At 80% and 90% fines, coat weights beyond ~6 g/m² result in high impermeability values with minimal further change, suggesting that

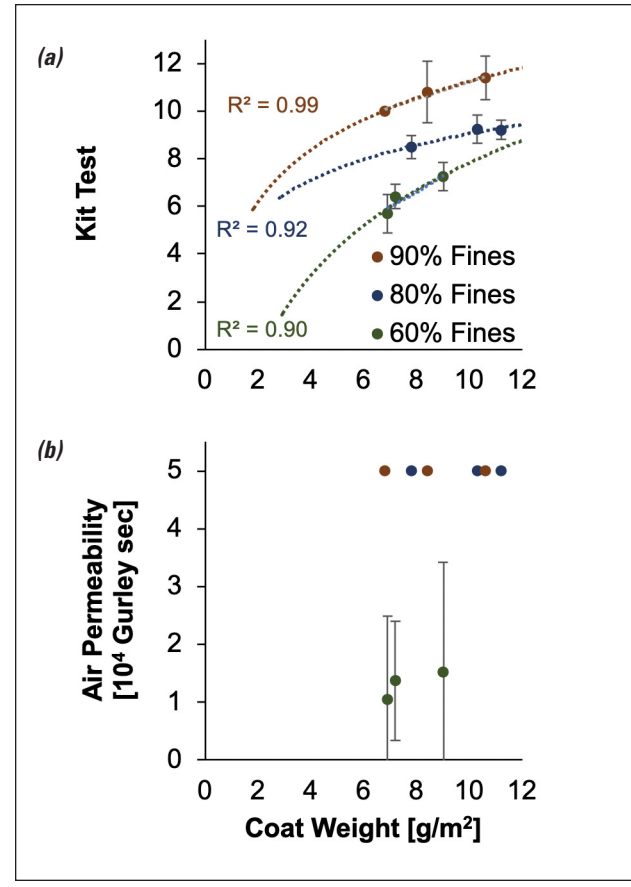

5. Relationship between coat weight and barrier performance with different fines content CNF: (a) Kit test values as a function of coat weight; and (b) air permeability (Gurley seconds × 10^4) as a function of coat weight. Data points are grouped according to the fines content used to develop the coating. Different coat weights were accomplished with the use of different solids contents (0.4%, 0.5%, and 0.6%).

maximum density is reached regardless of additional coating. By contrast, at 60% fines, air permeability still improves with increasing coat weight, showing that thickness plays a larger role when fines fraction is lower.

Taken together, these results show that similar barrier properties can be achieved, either through higher fines content at lower coat weight or through additional coat weight at lower fines content. From an industrial perspective, this flexibility provides opportunities for cost optimization: because high fines contents are more expensive to produce, applying slightly higher coat weights with lower fines suspensions may reach equivalent barrier performance. Thus, CNF barrier coatings can be tailored not only to technical targets but also to economic constraints, broadening the options for scalable production.

CONCLUSION

This work demonstrates the development and validation of a laboratory-scale vacuum-assisted coating system capable of producing CNF barrier coatings on paper. Experiments revealed that vacuum assistance significantly increases sol-

ids content prior to thermal drying, thereby reducing drying demand and improving coating efficiency. The results also confirm what others have reported — that the maximum coat weight that can be obtained without vacuum is around 2 g/m², but with vacuum, coat weights much higher than 5 g/m² can be obtained in a single pass.

The coat weight can be tuned by multiple independent process variables, including solids concentration, rod displacement, web speed, and filtration length before the rod. The coat weight changes are reliably captured by a predictive mathematical model. The agreement between model predictions and experimental results confirms the feasibility of forecasting coat weights under diverse process conditions.

Barrier testing further demonstrated that while higher coat weights generally improve grease and air resistance, the process route used to reach a given coat weight can influence final performance. Thus, coat weight is necessary, but not sufficient, to describe functionality, and understanding how operational parameters affect coating structure is critical for reliable property control. The barrier properties can be obtained with lower fines content, provided that coat weight is adjusted accordingly.

Overall, these findings provide a technical framework for advancing CNF barrier coatings toward industrial implementation. By combining predictive modeling, tunable processing, and flexible property optimization strategies, vacuum-assisted CNF coating offers a potential path to generate a paper grade that has a layer of CNF. **TJ**

ACKNOWLEDGMENTS

The authors thank Wyatt Fessler, Kyle Guerette, Zach Applebee, and Liza White for technical support and the University of Maine Process Development Center for equipment use. This work was supported by the University of Maine Sea Grant (NA23OAR4170178-T1-01), the University of Maine Institute of Medicine, and a Flagship Fellowship, as well as by the Maine Space Grant Consortium (SG-22-25), National Science Foundation (PFI-RP #2234150), and the National Institutes of Health (#R01DK128805). Materials were donated by Sappi North America and Kruger Canada.

LITERATURE CITED

1. Yi, T., Zhao, H., Mo, Q., et al., *Materials* 13(22): 5062(2020). https://doi.org/10.3390/ma13225062.
2. Zeng, J., Zeng, Z., Cheng, Z., et al., *Sci. Rep.* 11(1): 11918(2021). https://doi.org/10.1038/s41598-021-91420-y.
3. Kim, G.-H., Kang, D.-H., Jung, B.-N., et al., *Polymers* 14(4): 833(2022). https://doi.org/10.3390/polym14040833.
4. Huang, S., Wang, X., Zhang, Y., et al., *Sci. Rep.* 12(1): 16148(2022). https://doi.org/10.1038/s41598-022-20499-8.
5. "The Process Development Center: Nanocellulose," Process Development Center, University of Maine, Orono, ME, USA. Available [Online] https://umaine.edu/pdc/nanocellulose-2/ <17Nov2025>.
6. Hossain, R., Tajvidi, M., Bousfield, D., et al., *Carbohydr. Polym.* 267: 118221(2021). https://doi.org/10.1016/j.carbpol.2021.118221.
7. Prasad, S., Dave, A., and Misra, S., in *Organic-Based Nanomaterials in Food Packaging* (K. Younis, O. Yousuf, and S. Ul Islam, Eds.), Springer Nature Switzerland, Cham, 2024.
8. Kumar, V., Bollström, R., Yang, A., et al., *Cellulose* 21(5): 3443(2014). https://doi.org/10.1007/s10570-014-0357-5.
9. Du, Y., Liu, J., Wang, J., et al., *Pap. Biomater.* 2(2): 26(2017). https://doi.org/10.26599/PBM.2017.9260011.
10. Mele, G., Bloise, E., Cosentino, F., et al., *ACS Omega* 4(1): 718(2019). https://doi.org/10.1021/acsomega.8b02880.
11. Helanto, K., Talja, R., Li, S., et al., *Nord. Pulp Pap. Res. J.* 37(1): 108(2022). https://doi.org/10.1515/npprj-2021-0070.
12. Fein, K., Bousfield, D.W., and Gramlich, W.M., *ACS Appl. Polym. Mater.* 3(7): 3666(2021). https://doi.org/10.1021/acsapm.1c00620.
13. Zier, S., White, L.R., Johnstone, D., et al., *Langmuir* 41(9): 26751(2025). https://doi.org/10.1021/acs.langmuir.5c03185.
14. Qureshi, W.A., Radjarejesri, S., Shanmugam, K., et al., *J. Nanomater.* 2022(1): 9481983(2022). https://doi.org/10.1155/2022/9481983.
15. Yook, S., Park, H., Park, H., et al., *Cellulose* 27(8): 4509(2020). https://doi.org/10.1007/s10570-020-03061-5.
16. Aulin, C. and Ström, G., *Ind. Eng. Chem. Res.* 52(7): 2582(2013). https://doi.org/10.1021/ie301785a.
17. Lavoine, N., Desloges, I., Khelifi, B., et al., *J. Mater. Sci.* 49(7): 2879(2014). https://doi.org/10.1007/s10853-013-7995-0.
18. Afra, E., Mohammadnejad, S., and Saraeyan, A., *Prog. Org. Coat.* 101: 455(2016). https://doi.org/10.1016/j.porgcoat.2016.09.018.
19. Yselaure, B., "MFC for paper surface treatment," Master's thesis, Luleå University of Technology, Luleå, Sweden, 2017.
20. Kumar, V., Koppolu, V.R., Bousfield, D., et al., *Cellulose* 24(3): 1247(2017). https://doi.org/10.1007/s10570-017-1201-5.
21. Matikainen, L., "Nanocellulose as barrier coating deposited using a laboratory rod coater," Master's thesis, Aalto University, Espoo, Finland, 2017.
22. Mazhari Mousavi, S.M., Afra, E., Tajvidi, M., et al., *Cellulose* 24(7): 3001(2017). https://doi.org/10.1007/s10570-017-1299-5.
23. Tyagi, P., Lucia, L.A., Hubbe, M.A., et al., *Carbohydr. Polym.* 206: 281(2019). https://doi.org/10.1016/j.carbpol.2018.10.114.
24. Saini, S., Kardam, S.K., Kadam, A.A., et al., *Prog. Org. Coat.* 165: 106747(2022). https://doi.org/10.1016/j.porgcoat.2022.106747.
25. Jo, H.M., Kim, D.H., Lee, S.H., et al., *BioResources* 17(4): 6222(2022). https://doi.org/10.15376/biores.17.4.6222-6233.
26. Fillat, Ú., Vergara, P., Villar, J.C., et al., *Prog. Org. Coat.* 179: 107543(2023). https://doi.org/10.1016/j.porgcoat.2023.107543.
27. Richmond, F., "Cellulose nanofibers use in coated paper," Ph.D. thesis, University of Maine, Orono, ME, USA, 2014.
28. Haavisto, S., Salmela, J., Jäsberg, A., et al., *TAPPI J.* 14(5): 291(2015). https://doi.org/10.32964/10.32964/TJ14.5.291.
29. Kinnunen-Raudaskoski, K., Hjelt, T., Forsström, U., et al., *TAPPI J.* 16(4): 179(2017). https://doi.org/10.32964/TJ16.4.179.

30. Kumar, V., Ottesen, V., Syverud, K., et al., *BioResources* 12(4): 7656(2017). https://doi.org/10.15376/biores.12.4.7656-7679.

31. Koppolu, R., Banvillet, G., Ghimire, H., et al., *ACS Appl. Nano Mater.* 5(8): 11302(2022). https://doi.org/10.1021/acsanm.2c02423.

32. Koppolu, R., Lahti, J., Abitbol, T., et al., *ACS Appl. Mater. Interfaces* 11(12): 11920(2019). https://doi.org/10.1021/acsami.9b00922.

33. Koppolu, R., Lahti, J., Abitbol, T., et al., *Cellulose* 30(11): 6945(2023). https://doi.org/10.1007/s10570-023-05281-x.

34. Tayeb, A.H., Tajvidi, M., Bousfield, D., *Molecules* 25(6): 1344(2020). https://doi.org/10.3390/molecules25061344.

35. Al-Gharrawi, M., Ollier, R., Wang, J., et al., *J. Coat. Technol. Res.* 19(1): 3(2022). https://doi.org/10.1007/s11998-021-00482-0.

36. Pokharel, K., Bousfield, D., and Wang, J., *TAPPI J.* 24(1): 36(2025). https://doi.org/10.32964/TJ24.1.36.

37. Al-Gharrawi, M.Z., Wang, J., and Bousfield, D.W., *BioResources* 16(2): 3285(2021). https://doi.org/10.15376/biores.16.2.3285-3297.

38. Tayeb, A.H., Tajvidi, M., and Bousfield, D., *Sustainable Chem.* 1(3): 198(2020). https://doi.org/10.3390/suschem1030014.

39. Zier, S., Hoeft, Z., Quinn, J.P.W., et al., *Cellulose* (2025). https://doi.org/10.1007/s10570-025-06838-8.

40. Mazhari Mousavi, S.M., Afra, E., Tajvidi, M., et al., *Prog. Org. Coat.* 122: 207(2018). https://doi.org/10.1016/j.porgcoat.2018.05.024.

ABOUT THIS PAPER

Cite this article as:
Zier, S., Hoeft, Z., Snape, J., et al., *TAPPI J.* 24(11): 541(2025). https://doi.org/10.32964/TJ24.11.541

DOI: https://doi.org/10.32964/TJ24.11.541

ISSN: 0734-1415

Publisher: TAPPI Press

About this journal

ABOUT THE AUTHORS

We studied this topic because there is a need to get CNF onto paper. Here, we show that a CNF layer on paper has great barrier properties. The most difficult aspects of this research were automation and repeatability. Through this study, we found that water removal is very difficult, but it was interesting to achieve good results even after double folding.

Mills might benefit from the information here when developing new grades of paper. Our next step is to take this method from laboratory to pilot scale.

Zier is a Ph.D. candidate and research assistant; Hoeft is a research assistant; Snape is a research assistant; Bousfield is professor; and Howell is professor at the University of Maine in Orono ME, USA. Email Bousfield at bousfld@maine.edu.

Zier

Hoeft

Snape

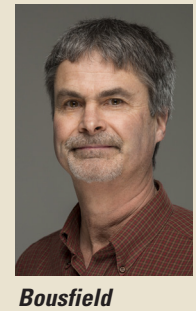

Bousfield

Howell